Supporting information

Qingshi Meng[a,#], Tengfei Chi[a,#], Shuang Guo[b], Milad Razbin,[c] Shuying Wu,[c] Shuai He,[d*]
Sensen Han[a,*], Shuhua Peng [d,*]

[a] College of Aerospace Engineering, Shenyang Aerospace University, Shenyang 110136, China

[b] Health Service Department, Northern Theatre General Hospital, Shenyang, 110016, China

[c] School of Aerospace, Mechanical and Mechatronic Engineering, The University of Sydney, Sydney, NSW 2006, Australia

[d] School of Mechanical and Manufacturing Engineering, The University of New South Wales, Sydney, NSW 2052, Australia

[*]Corresponding Author: Sensen Han, Shuai He, and Shuhua Peng

Email: sauhansen@163.com, shuai.he@unsw.edu.au, shuhua.peng@unsw.edu.au

[#]These authors contributed equally to this work.

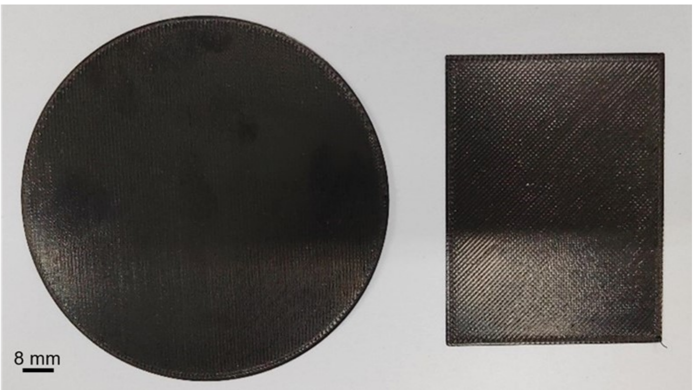

Figure S1. Image of 3D printing conductive films with thickness of 0.5 mm before cutting.

(a)

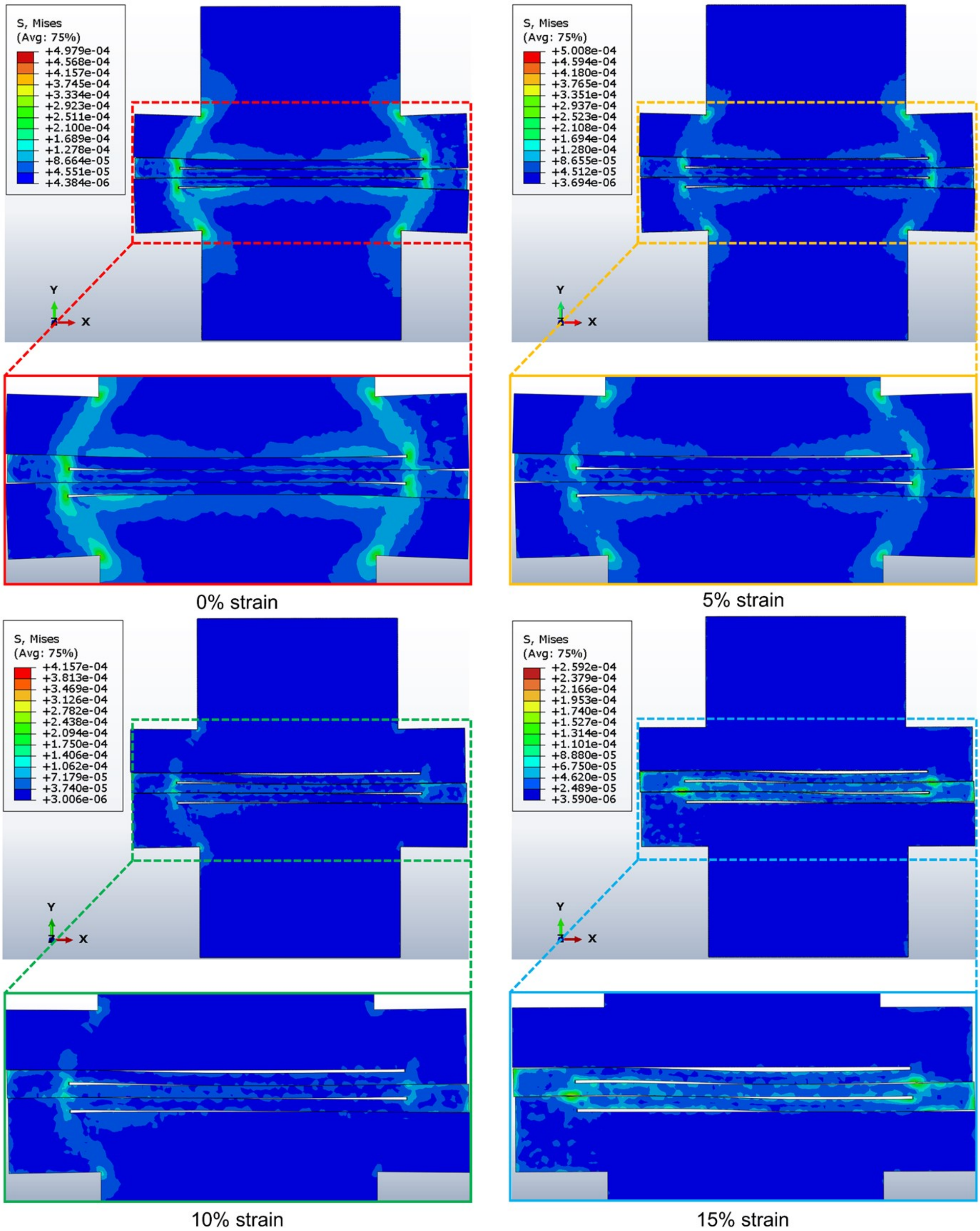
S, Mises
(Avg: 75%)
+4.979e-04
+4.568e-04
+4.157e-04
+3.745e-04
+3.334e-04
+2.923e-04
+2.511e-04
+2.100e-04
+1.689e-04
+1.278e-04
+8.664e-05
+4.551e-05
+4.384e-06
Y
X
0% strain
S, Mises
(Avg: 75%)
+5.008e-04
+4.594e-04
+4.180e-04
+3.765e-04
+3.351e-04
+2.937e-04
+2.523e-04
+2.108e-04
+1.694e-04
+1.280e-04
+8.655e-05
+4.512e-05
+3.694e-06
Y
X
5% strain
S, Mises
(Avg: 75%)
+4.157e-04
+3.813e-04
+3.469e-04
+3.126e-04
+2.782e-04
+2.438e-04
+2.094e-04
+1.750e-04
+1.406e-04
+1.062e-04
+7.179e-05
+3.740e-05
+3.006e-06
Y
X
10% strain
S, Mises
(Avg: 75%)
+2.592e-04
+2.379e-04
+2.166e-04
+1.953e-04
+1.740e-04
+1.527e-04
+1.314e-04
+1.101e-04
+8.880e-05
+6.750e-05
+4.620e-05
+2.489e-05
+3.590e-06
Y
X
15% strain

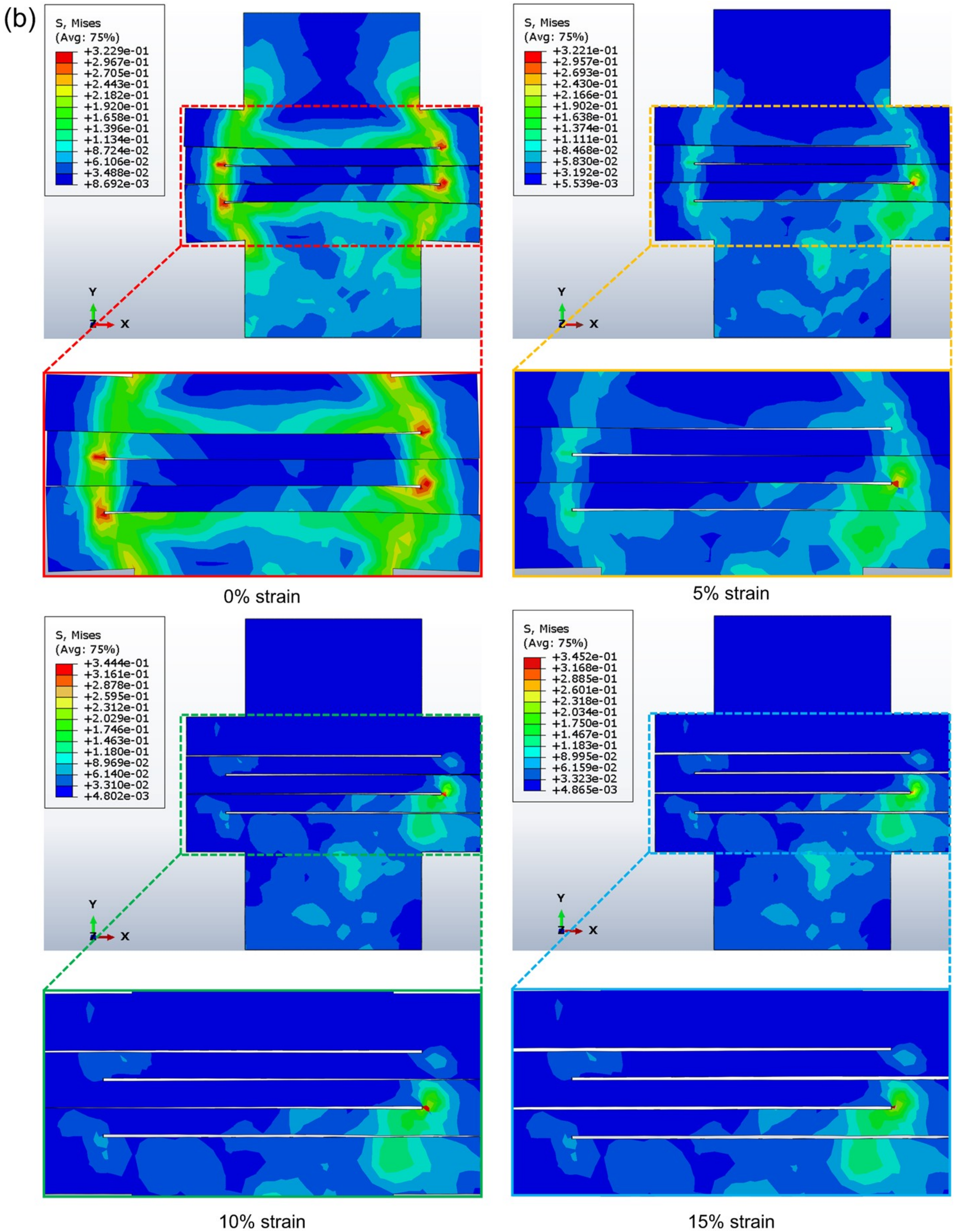

(b)
S, Mises
(Avg: 75%)
+3.229e-01
+2.967e-01
+2.705e-01
+2.443e-01
+2.182e-01
+1.920e-01
+1.658e-01
+1.396e-01
+1.134e-01
+8.724e-02
+6.106e-02
+3.488e-02
+8.692e-03
0% strain
S, Mises
(Avg: 75%)
+3.221e-01
+2.957e-01
+2.693e-01
+2.430e-01
+2.166e-01
+1.902e-01
+1.638e-01
+1.374e-01
+1.111e-01
+8.468e-02
+5.830e-02
+3.192e-02
+5.539e-03
5% strain
S, Mises
(Avg: 75%)
+3.444e-01
+3.161e-01
+2.878e-01
+2.595e-01
+2.312e-01
+2.029e-01
+1.746e-01
+1.463e-01
+1.180e-01
+8.969e-02
+6.140e-02
+3.310e-02
+4.802e-03
10% strain
S, Mises
(Avg: 75%)
+3.452e-01
+3.168e-01
+2.885e-01
+2.601e-01
+2.318e-01
+2.034e-01
+1.750e-01
+1.467e-01
+1.183e-01
+8.995e-02
+6.159e-02
+3.323e-02
+4.865e-03
15% strain

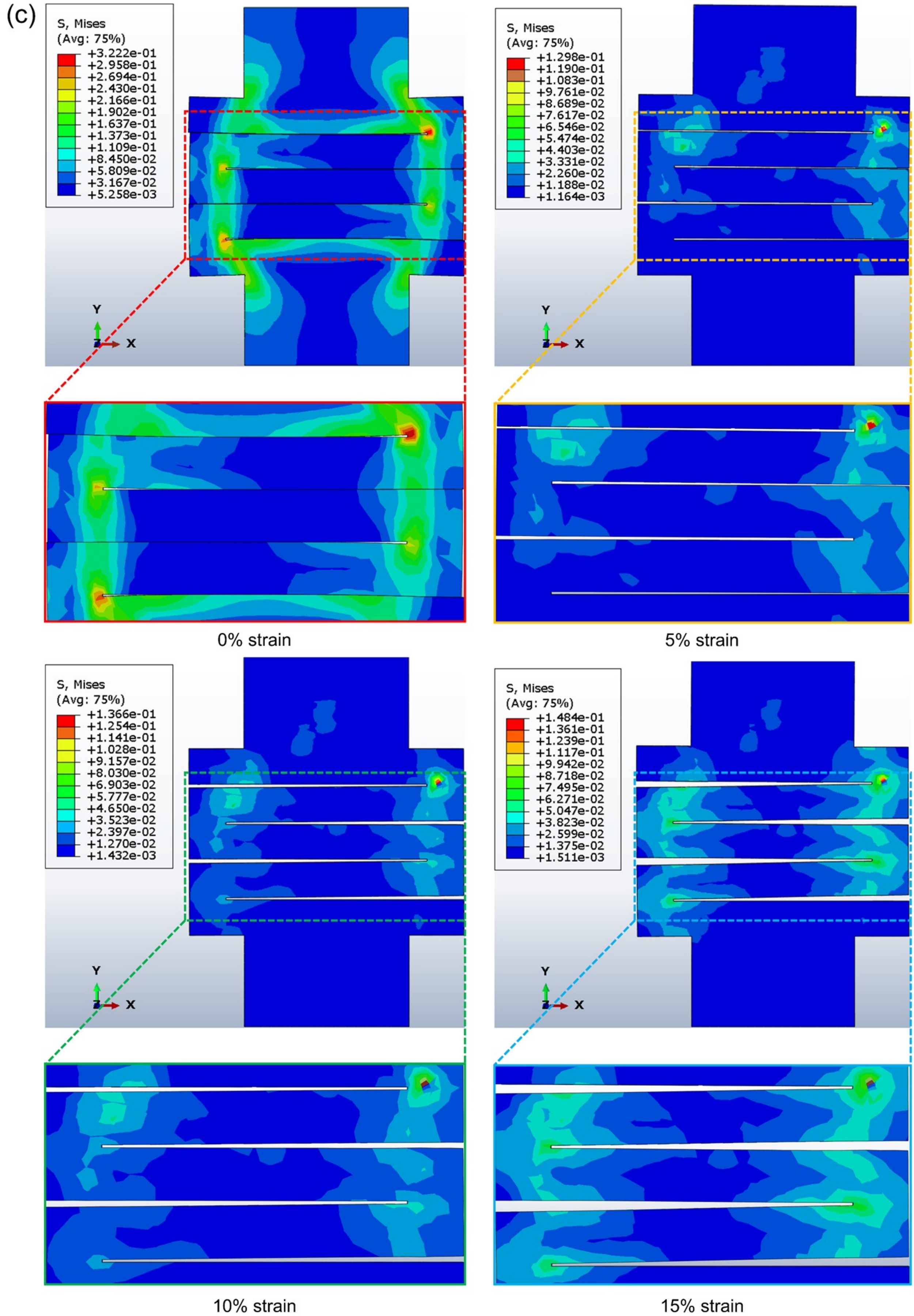

Figure S2. FEM analysis of strain sensors with different cutting pitch lengths between serpentine curves (p). a) The states of the sensor with p = 0.5 mm at 0% strain, 5% strain, 10% strain and 15%

strain. b) The states of the sensor with p = 1 mm at 0% strain, 5% strain, 10% strain and 15% strain. c) The states of the sensor with p = 2 mm at 0% strain, 5% strain, 10% strain and 15% strain.

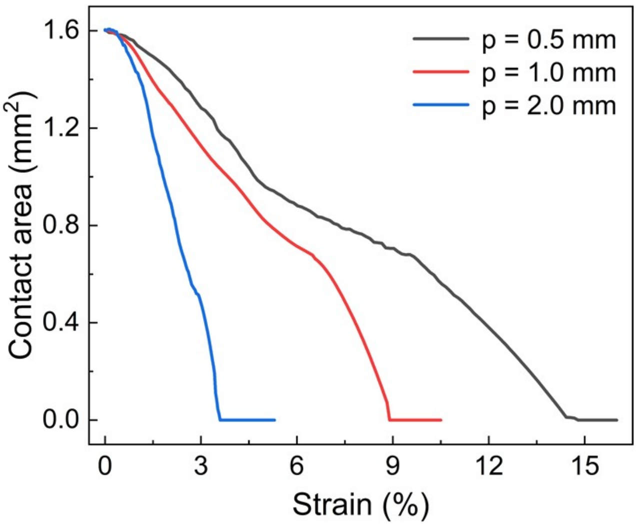

Figure S3. Corresponding contact area of one crack for the strain sensors with different cutting pitch lengths between serpentine curves (p) based on Figure S2.

Table S1 Comparisons with previous works in sensing mode

Transducing materials	Sensing modes	Gauge factor	Working range	Resistance relation to strain	Off-axis mode rejection	Temperature rejection	Reference
EGaIn	Strain	4.91	320%	Non-linear	Not shown	Insensitive to temperature (20~80℃)	[1]
MWCNT	Strain	56	70%	Non-linear	Insensitive to pressure	Not shown	[2]
rGo & Nano fiber	Strain	1.6(~10%); 7.1(~100%)	100%	Non-linear	Not shown	Not shown	[3]
AgNWs	Strain	7.5(~40%); 12(~100%)	100%	Non-linear (Two linear regions)	Not shown	Temperature changes by applying strain	[4]
Conductive yarns	Strain	49.5	100%	Linear	Insensitive to pressure and bending	Insensitive to temperature (23.2~40.1℃)	[5]
Nanographene	Strain	325	0.4%	Linear	Not shown	Not shown	[6]
CNT	Strain	8~207	50%	Non-	Not	Not shown	[7]

				linear (Three linear regions)	shown		
Conductive Composite Hydrogels	Strain & Pressure	3.4	300%	Linear		Not shown	[8]
Graphene composite	Strain & Pressure	＜15	100%	Non-linear (Three linear regions)		Not shown	[9]
Conductive TPU	Strain	500	10%	Linear	Insensitive to pressure, bending and twisting	Insensitive to temperature (20~80℃)	This work

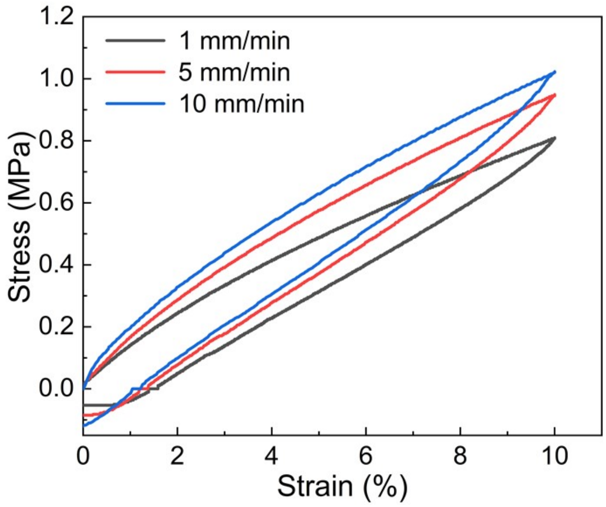

Figure S4. The mechanical hysteresis of the sensor under varying stretching speeds of 1 mm/min, 5 mm/min, and 10 mm/min

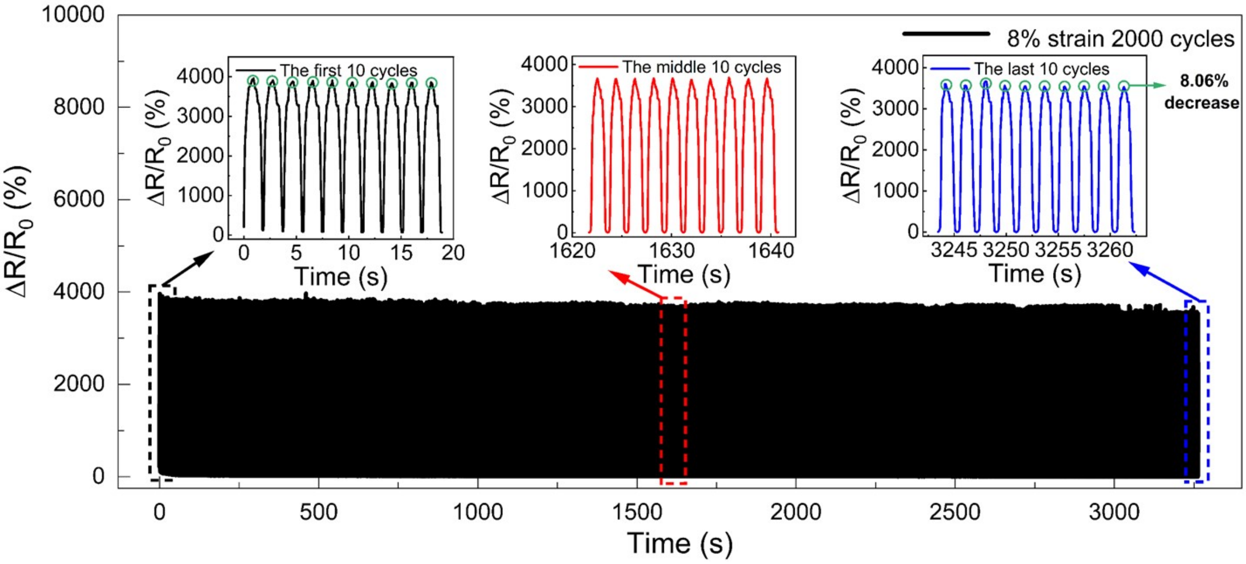

Figure S5. Sensor stability study over 2000 cycles at peak strain of 8%. The insets showing the first 10 cycles, middle 10 cycles, and last 10 cycles, respectively.

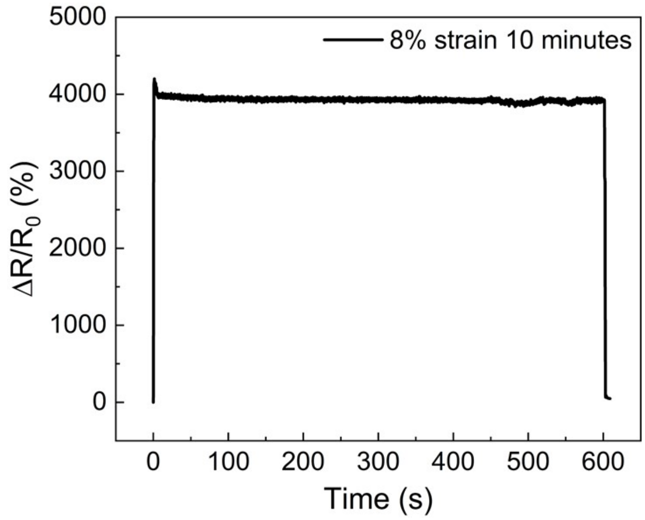

Figure S6. The resistance response of the sensor when subjected to a static 8% strain for more than 10 minutes.

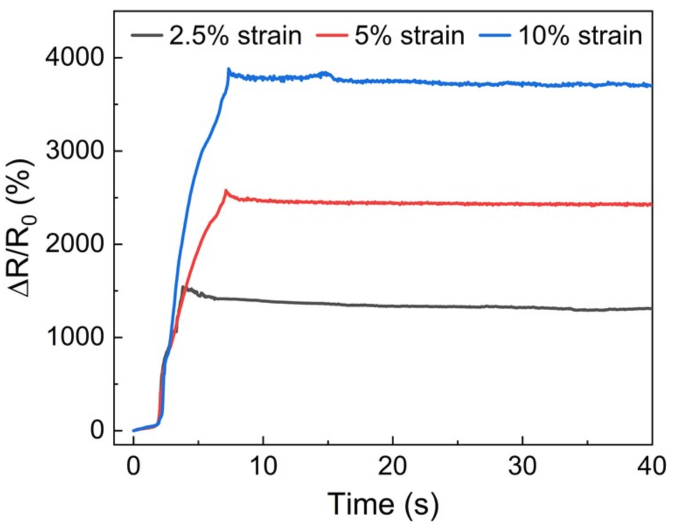

Figure S7. The relative resistance change of the sensor with a step strain to show low creep and static stability.

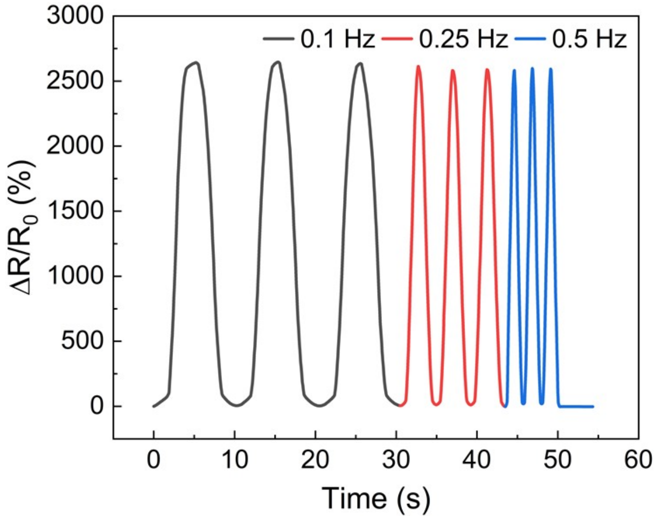

Figure S8. Dynamic stability of the sensor at various frequencies ranging from 0.1 to 0.5 Hz.

References:

1 J. Chen, J. Zhang, Z. Luo, J. Zhang, L. Li, Y. Su, X. Gao, Y. Li, W. Tang, C. Cao, Q. Liu, L. Wang and H. Li, ACS Appl. Mater. Interfaces, 2020, 12, 22200-22211.

2 J. Oh, J. C. Yang, J.-O. Kim, H. Park, S. Y. Kwon, S. Lee, J. Y. Sim, H. W. Oh, J. Kim and S. Park, ACS Nano, 2018, 12, 7546-7553.

3 C. Yan, J. Wang, W. Kang, M. Cui, X. Wang, C. Y. Foo, K. J. Chee and P. S. Lee, Adv. Mater., 2013, 26, 2022-2027.

4 G. Lee, G. Y. Bae, J. H. Son, S. Lee, S. W. Kim, D. Kim, S. G. Lee and K. Cho, Adv. Sci., 2020, 7, 2001184.

5 Z. Liu, Y. Zheng, L. Jin, K. Chen, H. Zhai, Q. Huang, Z. Chen, Y. Yi, M. Umar, L. Xu, G. Li, Q. Song, P. Yue, Y. Li and Z. Zheng, Adv. Funct. Mater., 2021, 31, 2007622.

6 J. Zhao, C. He, R. Yang, Z. Shi, M. Cheng, W. Yang, G. Xie, D. Wang, D. Shi and G. Zhang, Appl. Phys. Lett., 2012, 101, 063112.

7 Y. Wang, F. Wang, S. Yazigi, D. Zhang, X. Gui, Y. Qi, J. Zhong and L. Sun, Carbon, 2021, 173, 849-856.

8 H. Wei, D. Kong, T. Li, Q. Xue, S. Wang, D. Cui, Y. Huang, L. Wang, S. Hu, T. Wan and G. Yang, ACS Sens., 2021, 6, 2938-2951.

9 J. Wang, C. Zhang, D. Chen, M. Sun, N. Liang, Q. Cheng, Y. Ji, H. Gao, Z. Guo, Y. Li, D. Sun, Q. Li and H. Liu, ACS Appl. Mater. Interfaces, 2020, 12, 51854-51863.